

# A tert-butyl functionalized quinone as active material for rechargeable aqueous zinc-ion batteries exhibiting high round-trip efficiency

Alejandra Ibarra Espinoza <sup>a</sup>, Thomas J. Baker <sup>a</sup>, Storm W.D. Gourley <sup>a</sup>, Caio M. Miliante <sup>b</sup>, Kevin J. Sanders <sup>c</sup>, Zeyuan Liu <sup>c</sup>, Gillian R. Goward <sup>c</sup>, Oleg Rubel <sup>b</sup>, Brian D. Adams <sup>a,d,\*</sup>, Drew Higgins <sup>a,\*\*</sup>

<sup>a</sup> Department of Chemical Engineering, McMaster University, 1280 Main Street West, Hamilton, Ontario L8S 4L7, Canada

<sup>b</sup> Department of Materials Science and Engineering, McMaster University, 1280 Main Street West, Hamilton, Ontario L8S 4L7, Canada

<sup>c</sup> Department of Chemistry and Chemical Biology, McMaster University, 1280 Main Street West, Hamilton, Ontario L8S 4L7, Canada

<sup>d</sup> Salient Energy Inc., 21 McCurdy Ave, Dartmouth, Nova Scotia B3B 1C4, Canada

## ARTICLE INFO

### Keywords:

Zinc-ion battery  
ZIB  
Quinone  
Aqueous battery

## ABSTRACT

The implementation of renewable electricity into the grid requires efficient grid-energy storage systems for balancing supply and demand. Rechargeable zinc-ion batteries (ZIBs) are a low-cost, safe option for grid energy storage; however, challenges pertaining to energy storage capacity, round-trip efficiency, stability, and reliance on critical minerals still need to be addressed. Herein, 3,5-di-tert-butyl-ortho-benzoquinone (TBOBQ) was evaluated as an organic cathode material for ZIBs, achieving a maximum theoretical specific capacity of 246 mAh/g at 40 mA/g (C/4) with a 1 to 1 mass ratio of TBOBQ-to-acetylene black. The observed charge and discharge curves presented a voltage hysteresis of only 100 mV, resulting in a round-trip efficiency of 90 %. Degradation of the TBOBQ cathode was attributed to fractional dimerization and dissolution during discharge, as observed by nuclear magnetic resonance, mass spectroscopy, and rotating ring disk electrode. This work sets the stage for the development of organic ZIB cathodes based on TBOBQ with high discharge capacities and energy efficiency.

## Introduction

As global electricity demand continues to increase year over year, society's reliance on the combustion of fossil fuels to meet this rising demand causes environmental repercussions that are no longer just a concern but are a sign for immediate, necessary change. Renewable energy sources (*i.e.*, wind and solar) are well-positioned to replace entrenched fossil fuels in the power sector [1,2]. However, the variable nature of wind and solar energy production hinders their integration into the current electrical grid infrastructure and necessitates the development and use of stationary energy storage systems [1–3]. Rechargeable zinc-ion batteries (ZIBs) are a type of electrochemical energy storage with a working principle based on the reversible migration of  $Zn^{2+}$  cations from the anode to the cathode, similar to lithium-ion batteries (LIBs) that utilize  $Li^+$  [4]. ZIBs have the potential to be deployed for stationary energy storage applications owing to their

attractive characteristics, such as high safety, low cost, and low environmental impact [3]. ZIBs use an aqueous electrolyte alongside abundant, non-toxic zinc metal anodes with a low redox potential (-0.76 V vs SHE) and high theoretical capacity (820 mAh/g) [4,5]. The stability of metallic zinc in the presence of water is an added advantage, since the use of aqueous electrolytes lowers the cost, simplifies manufacturing, and increases safety [6]. Although ZIBs offer many advantages, a fundamental challenge in their development is the lack of high-capacity, energy-efficient, and stable cathode materials [7] that can withstand repeated charge/discharge cycles at rates appropriate for grid-scale energy storage (*i.e.*, 4–6 h of energy storage [3]). Materials like Mn-based oxides [8], V-based oxides [9], Mo-based oxides [10], and Prussian blue analogs [11] have been explored as cathode materials for ZIBs [5,7]. Nevertheless, the stability of inorganic cathodes is hindered by metal dissolution and structural degradation, leading to poor battery lifetimes [12,13].

\* Corresponding author at: Department of Chemical Engineering, McMaster University, 1280 Main Street West, Hamilton, Ontario L8S 4L7, Canada.

\*\* Corresponding author.

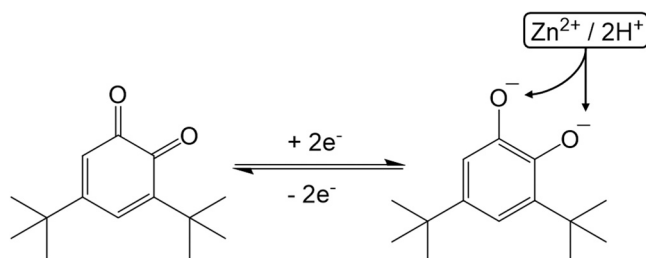
E-mail addresses: [adamsb13@mcmaster.ca](mailto:adamsb13@mcmaster.ca) (B.D. Adams), [higgid2@mcmaster.ca](mailto:higgid2@mcmaster.ca) (D. Higgins).

On the other hand, organic materials with redox-active functional groups have attracted attention for use as cathodes in ZIBs due to their high theoretical capacity and the ability to functionalize the organic structures to modulate solubility, reversible charge/discharge potentials, and improve stability [14–17]. Moreover, organic electrode materials rely on inexpensive and earth-abundant elements, avoiding the need for energy-intensive and environmentally destructive extraction and refining of critical minerals [18]. Of particular interest are quinones, organic structures with two redox-active carbonyl groups in the ortho or para positions of an unsaturated six-carbon ring structure [19] that can interact with metallic cations such as  $Zn^{2+}$  [17,20]. Different quinone structures have been tested as cathodes for aqueous ZIBs, including tetraamino-p-benzoquinone (TABQ), showing a discharge capacity of 303 mAh/g at a rate of 0.1 A/g with an average discharge voltage of ca. 0.9 V vs  $Zn^0/Zn^{2+}$  and a voltage difference between the charge and discharge curves of ca. 120 mV [21].

Despite promising results from early studies, there are several challenges facing the utilization of quinone molecules in ZIBs [22,23]. First, organic cathodes have relatively low electrical conductivity when compared to metal oxides, requiring higher amounts of conductive additives (*i.e.*, carbon materials like acetylene black), thereby reducing the energy density of the electrode [24,25]. Additionally, capacity fade can be caused by irreversible decomposition reactions among quinone molecules or with the surrounding materials, especially at radical intermediate states of the carbonyl groups (like  $\bullet C-O^-$ ), that are formed during multistep discharge processes [18]. As such, elucidating the unknown degradation mechanisms of organic cathodes can provide insights for the design and development of new organic cathode materials with high capacity and stability.

3,5-di-tert-butyl-o-benzoquinone (TBOBQ) is a particularly promising quinone with two carbonyl groups in the ortho position and two tert-butyl structures attached to the aromatic ring (**Scheme 1, left**). Park *et al.* [26] showed the capability of the carbonyl groups of TBOBQ for shuttling lithium ions for the re-lithiation of end-of-life LIBs cathodes, demonstrating the capacity of TBOBQ for coordinating and storing cations. Despite ZIBs using a different cation than lithium, TBOBQ can be considered for ZIBs thanks to the cation interchangeability of organic molecules [17].

To expand the current knowledge of organic cathode materials for aqueous ZIBs, this work develops an organic cathode based on TBOBQ and explores the electrochemical properties and the mechanisms responsible for energy storage and degradation. The galvanostatic charge/discharge curves of the TBOBQ cathode showed a deliverable discharge capacity of 246 mAh/g at a current density of 40 mA/g. Furthermore, the charge/discharge curves of TBOBQ showed flat voltage plateaus separated by only 100 mV. The small separation between voltage plateaus, or voltage hysteresis, contributes to a round-trip efficiency (RTE) of 90 %. Low RTE represents energy losses during charge/discharge, which has an economic cost [27] and can lead to undesired heat generation. Characterization of the energy storage mechanism through Fourier transform infrared spectroscopy (FTIR), X-ray diffraction spectroscopy (XRD), and inductively coupled plasma optical emission spectroscopy (ICP-OES), and CHNS elemental analysis



**Scheme 1.** Redox reaction of TBOBQ where 2 electrons get stored in the oxygen atoms due to their higher electronegativity.

(CHNS-EA) showed that the interaction of carbonyl groups with  $Zn^{2+}$  and  $H^+$  from the electrolyte contributes to the energy storage capabilities of the TBOBQ cathode. Finally, capacity fade in the TBOBQ-based electrodes over repeated charge/discharge cycles was attributed to active material dissolution alongside the formation of a high molecular weight degradation product identified by gas chromatography-mass spectroscopy (GC-MS). This work contributes to the development of ZIBs through the exploration of novel cathode materials with high discharge capacity at a voltage above 1 V vs  $Zn^0/Zn^{2+}$  alongside a low voltage hysteresis that benefits the round-trip efficiency. Additionally, the materials characterization and elucidation of degradation mechanisms provide fundamental insight that can guide the development of improved performance and stability of TBOBQ or other organic molecule-based cathodes for ZIBs.

## Methodology

### Electrochemical measurements

All materials were used as purchased, with no further modification. The cathodes were prepared using a weight ratio of 45:45:10 of TBOBQ (Sigma Aldrich), acetylene black (TIMCAL), and poly(vinylidene difluoride) (PVDF) (Alfa Aesar) binder, respectively, mixed in a 1-methyl-2-pyrrolidinone (NMP) (Sigma Aldrich) based slurry. The cathode with this composition is hereafter referred to as TBOBQ-441. To prepare the cathodes, the powders and solvent mixture were mixed in a planetary mixer (Mazerustar KK-250S) for 5 min to form a slurry, which was then cast onto a carbon paper current collector to a thickness of 250 micrometers, followed by drying for 24 h at room temperature. The average mass loading of TBOBQ in the cathode was 0.83 mg/cm<sup>2</sup>. TBOBQ:acetylene black:PVDF weight ratios of 60:30:10 and 80:10:10 (hereafter referred to as TBOBQ-631 and TBOBQ-811, respectively), were used to evaluate the effect of the TBOBQ-to-acetylene black ratio on the performance of the battery. The electrochemical characterizations described next were performed at room temperature. CR2032-coin cells were used for the galvanostatic charge and discharge measurements (GCD) using zinc foil (0.008", McMaster-Carr) as the anode, a glass fiber separator (grade GF/D, Whatman), 0.5" diameter cathode, and 150 microliters of 1 M  $ZnSO_4$  solution as the electrolyte. In the GCD test, the open circuit voltage (OCV) of the battery was allowed to stabilize during a 3-hour rest step, followed by a discharge and then a charge at a constant current density of 40 mA/g. All current densities and capacities described are normalized by the mass of TBOBQ in the cathode. Since ZIBs were assembled at a fully charged state, the coulombic efficiency (CE) was determined by the ratio of the discharge capacity to the subsequent charge capacity.

Cyclic voltammetry (CV) measurements were performed using a VSP-300 Biologic potentiostat in coin cells prepared with the procedure previously described. The working electrode potential window was from 0.8 V to 1.5 V vs  $Zn^0/Zn^{2+}$  with scan rates of 5, 6, 7, 8, 9, and 10 mV/s. To explore the stability of the TBOBQ-based electrodes over several discharge/charge cycles, the coin cell batteries were cycled at a current density of 100 mA/g. For evaluating the charge transfer resistance of the TBOBQ cathodes, electrochemical impedance spectroscopy (EIS) measurements were performed in the frequency range of 1 MHz to 100 mHz. The diffusion coefficient of  $Zn^{2+}$  in the electrode was measured by the galvanostatic intermittent titration technique (GITT) using a current pulse of 40 mA/g for 2 min, followed by a relaxation time of 30 min until reaching the final charge or discharge voltage. The diffusion coefficient for  $Zn^{2+}$  was estimated by the following Eq. (1) [28,29]:

$$D_{Zn} = \frac{4}{\pi \tau} \left( \frac{m_B * v_m}{M_B * S} \right)^2 \left( \frac{\Delta E_s}{\Delta E_r} \right)^2 \quad (1)$$

Where  $m_B$ ,  $M_B$ ,  $v_m$ , and  $S$  are the mass, molar mass, molar volume, and surface area of TBOBQ, respectively.  $\Delta E_s$ ,  $\Delta E_r$ , and  $\tau$  are the overvoltage

over the current pulse, the change in voltage over the rest time, and the time of the current pulse, respectively. The self-discharge test consisted of 20 conditioning cycles, and a 24-hour rest at OCV, followed by a full discharge/charge.

Measurements of electrolyte pH to explore the possible contribution of  $\text{H}^+$  in the storage mechanism were performed in a UV-vis cuvette cell using bromocresol green (Ricca) as a pH indicator. An 8 × 60 mm sheet cathode containing TBOBQ or 3,5-di-tert-butylcatechol (TBC) as active material prepared using the doctor blade technique as in the coin cell electrodes was used as the cathode along with a zinc foil anode and 1 M  $\text{ZnSO}_4$  electrolyte. The cathodes were charged and discharged with a current of 0.08 mA, and the changes in the electrolyte pH were observed visually.

For detecting dissolved species of TBOBQ during the discharge process, rotating ring disk electrode (RRDE) tests were performed using a Pine Research rotator and VSP-300 Biologic potentiostat. The RRDE tip consisted of a glassy carbon electrode of 5 mm in diameter and a Pt ring electrode around it, spaced 1.5 mm from the disk. An ink was prepared using 20  $\mu\text{L}$  of Nafion 117 (Sigma Aldrich, ca. 5 % in a mixture of lower aliphatic alcohols and water), 2.13 mg of acetylene black, and 2.13 mg of TBOBQ in 2 mL of 50 vol% ethanol and 50 vol% Millipore Type I Ultrapure water. The disk electrode was coated with the ink previously described by drop casting until a loading of 0.54 mg/cm<sup>2</sup> of TBOBQ was achieved. Zinc foil served as counter and reference electrodes. RRDE measurements were run at 900 rpm with a 0.1 M  $\text{ZnSO}_4$  electrolyte saturated with Ar. Linear sweep voltammetry was applied on the disk electrode from OCV to 0.8 V vs  $\text{Zn}^0/\text{Zn}^{2+}$  at a scan rate of 1 mV/s, while the Pt ring was kept at 1.5 V vs  $\text{Zn}^0/\text{Zn}^{2+}$ .

### Characterization

The infrared spectrum was obtained on a Nicolet Fourier-Transform Infrared (FTIR) Spectrometer (Model 6700) at a spectrum range of 4000–500 cm<sup>-1</sup>. Scanning electron microscopy (SEM) imaging and energy dispersive X-ray spectroscopy (EDS) characterization were conducted using a Thermo Scientific Quattro ESEM at the Canadian Centre for Electron Microscopy (CCEM) at McMaster University. A Bruker D8 DISCOVER with a Cu-K $\alpha$  radiation source with a wavelength of 1.5406 Å was employed at the McMaster Analytical X-Ray Diffraction Facility for the X-ray diffraction (XRD) measurements. The scans were processed on a 2θ range of 5–90 degrees. Inductive coupled plasma optical emission spectroscopy (ICP-OES) was carried out in an Agilent 5800 instrument. The discharged electrode samples were washed with Millipore Type I Ultrapure water to remove the remaining  $\text{ZnSO}_4$  electrolyte, then digested in concentrated  $\text{HNO}_3$  at 80 °C for 5 days. An Elementar CHNS/O Unicube elemental analysis (CHNS-EA) instrument was employed for quantifying S in discharged electrodes previously washed with Millipore Type I Ultrapure water to remove residual  $\text{ZnSO}_4$  electrolyte. The weight percentage of  $\text{Zn}^{2+}$  and S obtained from ICP-OES and CHNS-EA, respectively, were based on the weight of slurry of the cathode sample.

Liquid <sup>1</sup>H Nuclear magnetic resonance (<sup>1</sup>H NMR) spectra were collected using a Bruker Avance NEO spectrometer operating at a <sup>1</sup>H Larmor frequency of 600.13 MHz, corresponding to an external magnetic field strength of 14.1 T. Deuterated dimethyl sulfoxide (d6-DMSO) was used as the solvent. The TBOBQ cathodes studied by <sup>1</sup>H NMR were prepared by casting the TBOBQ active material onto carbon paper and cycled in a UV-Vis cuvette cell with metallic zinc as the negative electrode and 1 M  $\text{ZnSO}_4$  in D<sub>2</sub>O solvent electrolyte. After cycling, electrodes were removed from the cell, dried, and dissolved in d6-DMSO. Aliquots of electrolyte were also removed and studied by <sup>1</sup>H NMR. Gas chromatography-mass spectroscopy (GC-MS) studies were performed using an Agilent 6890–5973 gas chromatograph mass spectrometer using electron ionization on a cathode cycled 10 times.

### Theoretical methodology

Density functional theory (DFT) calculations were carried out utilizing the Gaussian 16 [30] package, with the B3LYP hybrid density functional [31] and the 6-311+G(d,p) basis set [32,33]. Geometry optimization was performed for all molecules. Stricter forces and step size cutoffs were considered for the optimization convergence by utilizing the “Opt=Tight” tag during geometry optimization, alongside a finer integration grid than the default (“Int=UltraFine” tag). The water solvation effect was also accounted for with an implicit solvation model (SMD) [34] to precisely capture the experimental conditions of the aqueous electrolyte. Vibrational frequency calculations were performed for all molecules to obtain their Gibbs free energy correction. No negative frequencies were found for the optimized structures. The binding energy ( $\Delta E_b$ , in eV) can be calculated by

$$\Delta E_b = G_{i_x-\text{TBOBQ}}^0 - \left( G_{\text{TBOBQ}}^0 + x * G_i^0 \right) \quad (2)$$

where  $G_{\text{TBOBQ}}^0$ ,  $G_{i_x-\text{TBOBQ}}^0$  and  $G_i^0$  are, respectively, the sum of electronic and thermal free energies of the TBOBQ molecule, the TBOBQ molecule with bonded  $i_x$  atoms, and of a single  $i$  ion,  $i$  is either  $\text{Zn}^{2+}$  or  $\text{H}^+$ , and  $x$  is the number of atoms being bonded to TBOBQ (1 for  $\text{Zn}^{2+}$  and 2 for  $\text{H}^+$ ). The electrostatic potential (ESP) analysis was performed using the Multiwfnn 3.7 program [35,36], with the VMD software [37] being used for plotting. A negative ESP value indicates a region with a concentration of electronic charges, while nuclear charges are predominant in regions with positive ESP values.

### Results and discussion

Cyclic voltammetry (CV) of TBOBQ-811 (whereby 811 indicates a TBOBQ, acetylene black, and PVDF weight ratio of 80:10:10) was performed to evaluate the electrochemical behavior of the TBOBQ cathode in the aqueous 1 M  $\text{ZnSO}_4$  electrolyte. The shape and position of the peaks in the CVs of TBOBQ-811 (Fig. 1a) were consistent as a function of cycle number, highlighting the electrochemical stability of TBOBQ under the measurement conditions employed and the reversibility of the desired redox reaction (Scheme 1) [38,39]. The peaks observed can be associated with the reduction and oxidation of the carbonyl groups in the TBOBQ molecule [19]. The reduction and oxidation of TBOBQ occurred within the electrochemical stability window of the 1 M  $\text{ZnSO}_4$  aqueous electrolyte, and thus, competition with the hydrogen evolution and oxygen evolution reactions is not of concern [40]. The kinetics of the TBOBQ oxidation and reduction were evaluated through the correlation between peak current ( $i$ ) and scan rate ( $v$ ) (Supplementary Discussion 1). As observed in Fig. 1b, the  $b$  value of the cathodic and anodic peaks had diffusion-controlled kinetics as the  $b$  value was close to 0.5 ( $b = 0.49$  for the cathodic peak;  $b = 0.57$  for the anodic peak). Diffusion-controlled kinetics indicate that the redox reactions take place in the bulk of the material, which requires positively charged ions,  $\text{Zn}^{2+}$  and  $\text{H}^+$ , to diffuse from the electrolyte into the matrix of the electrode for the energy storage to take place [41,42]. Additionally, the peaks in the CV of TBOBQ-811 showed a broad shape centered at ca. 1.03 V vs  $\text{Zn}^0/\text{Zn}^{2+}$  and ca. 1.25 V vs  $\text{Zn}^0/\text{Zn}^{2+}$ , for the cathodic and anodic peaks, respectively (Fig. 1a). The observed broad CV peaks could potentially be a consequence of the low conductivity of the electro-active materials, given the low content of conductive acetylene black within the TBOBQ-811 electrode (10 wt% of acetylene black), and the low conductivity of most quinone-containing organic molecules [25,43]. Hence, a CV experiment of a TBOBQ-441 cathode (with a weight ratio of TBOBQ, acetylene black, and PVDF of 45:45:10, respectively) was performed to investigate the electrochemical behavior of TBOBQ in an electrode formulation with higher conductivity. The CV curve obtained from TBOBQ-441, shown in Fig. S1, demonstrates a pair of cathodic peaks at 0.88 and 1.01 V vs  $\text{Zn}^0/\text{Zn}^{2+}$  and a pair of anodic peaks at 1.32

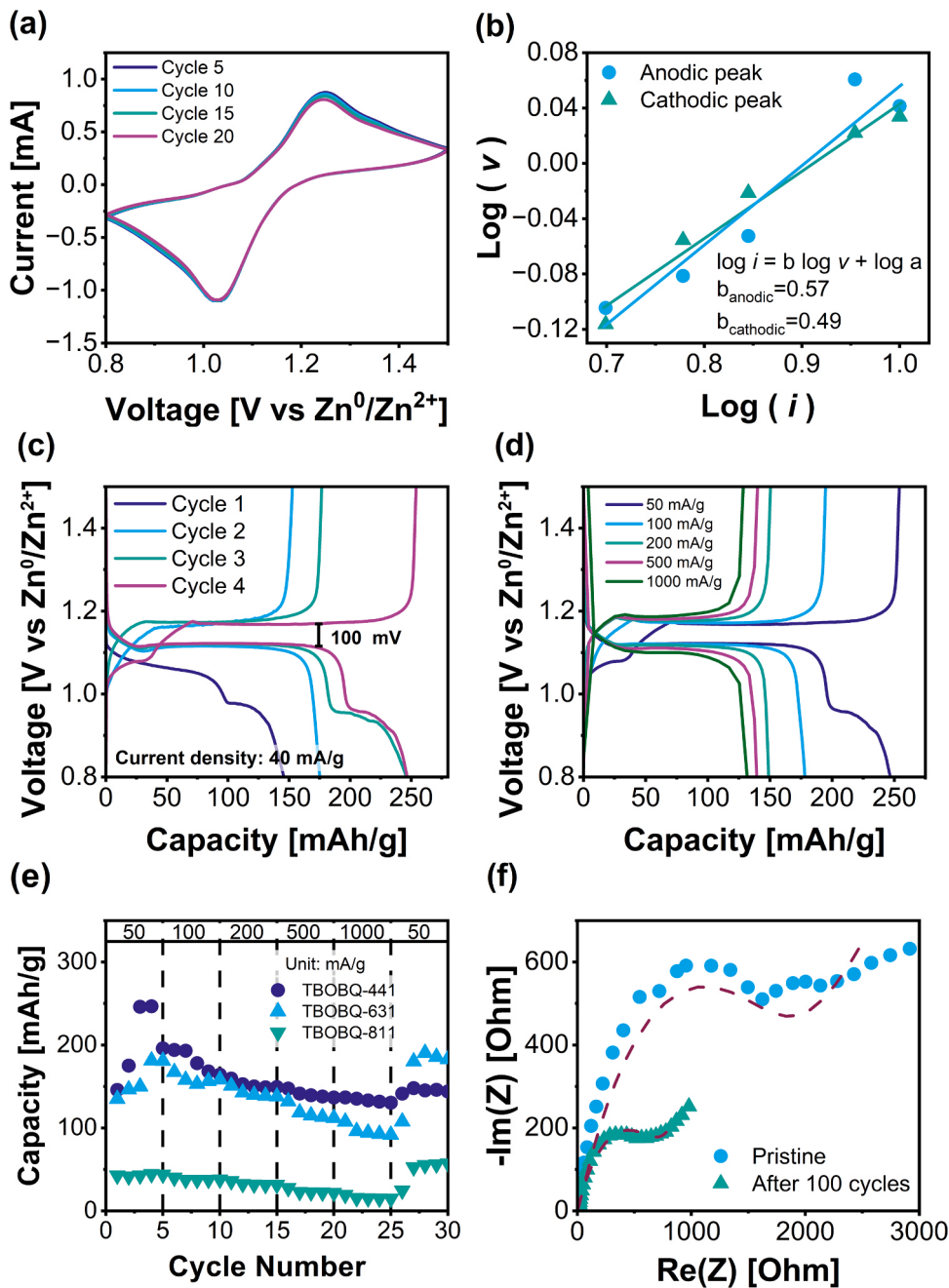


**Fig. 1.** Electrochemical characterization of TBOBQ cathodes; (a) CV curves of a TBOBQ-811 coin cell with 1 M ZnSO<sub>4</sub> electrolyte at different cycles at 10 mV/s. (b) Linear fitting of the peak currents and scan rate for obtaining the b-values. (c) Capacity curves of TBOBQ-441 at 40 mA/g (C/4) over the first 4 cycles. (d) Capacity curves of TBOBQ-441 at current densities of 50 (C/4), 100 (C/2), 200 (1.34 C), 500 (3.5 C), and 1000 mA/g (7.8 C). (e) Comparison of the rate capability of TBOBQ-441, TBOBQ-631, and TBOBQ-811 at current densities of 50 (C/4), 100 (C/2), 200 (1.34 C), 500 (3.5 C), 1000 (7.8 C) mA/g. (f) Nyquist plots of the impedance measurements of TBOBQ-811 and fitting of the impedance data in dashed lines. All current densities and capacities are normalized by the mass of TBOBQ.

and 1.41 V vs Zn<sup>0</sup>/Zn<sup>2+</sup>. The anodic and cathodic double peaks in the more conductive TBOBQ-441 CV result indicated that the broad peaks in the CV of TBOBQ-811 were each comprised of two electrochemical processes, which could not be clearly resolved in the TBOBQ-811 cathode formulation.

GDC testing was employed to evaluate the charge and discharge curves and capacities of the TBOBQ cathodes. The charge and discharge curve of TBOBQ-441 collected at a current density of 40 mA/g, shown in Fig. 1c, demonstrated a flat voltage plateau at 1.2 V and 1.1 V vs Zn<sup>0</sup>/Zn<sup>2+</sup>, respectively, that were in accordance with the anodic and cathodic peak at 1.32 and 1.01 V vs Zn<sup>0</sup>/Zn<sup>2+</sup>, respectively, observed in the CV curve of TBOBQ-441 (Fig. S1). A secondary discharge plateau

was observed at 0.95 V vs Zn<sup>0</sup>/Zn<sup>2+</sup> for cells tested under current densities below 100 mA/g. The secondary discharge plateau observed in Fig. 1c could be correlated to the broad peak at 0.88 V vs Zn<sup>0</sup>/Zn<sup>2+</sup> observed in the CV of TBOBQ-441 (Fig. S1). As discussed above, the CV of TBOBQ in an electrode formulation with a higher conductivity (like TBOBQ-441) showed two cathodic peaks (at 0.88 and 1.01 V vs Zn<sup>0</sup>/Zn<sup>2+</sup>). The presence of the secondary discharge plateau only at low current densities (as seen in Fig. 1d) could indicate that the electrochemical process represented by the mentioned plateau is kinetically limited. When the kinetics of an electrochemical process are inadequate for the current density applied to the battery, the kinetic limitations could hinder the transfer of Faradic current coming from the

electrochemical process [44]; hence, no additional discharge capacity is observed when cycling at current densities of 100 mA/g and higher (Fig. 1d). However, the specific mechanism underpinning this kinetically limited process is still unknown.

Additionally, the small voltage hysteresis of only 100 mV observed between the charge and discharge voltage plateaus is a measure of the voltage required for cathode discharge versus charge, and by extension, a gauge of the RTE [25,40,45]. Table 1 lists the discharge voltage at half-capacity, voltage hysteresis, RTE, and other important parameters describing the discharge behavior of several organic cathode materials reported in the literature. It can be observed that TBOBQ has a high discharge voltage compared to other organic cathodes, e.g., 3,4,9, 10-perylene-tetracarboxylicacid-dianhydride (0.4 V vs Zn<sup>0</sup>/Zn<sup>2+</sup>) [46] or pyrene-4,5,9,10-tetraone (0.7 V vs Zn<sup>0</sup>/Zn<sup>2+</sup>) [47], which results in an improved energy density of the TBOBQ cathodes (270 Wh/kg). Additionally, the voltage hysteresis of TBOBQ is among the lowest reported values (100 mV), compared to organic cathodes like 2,3,7, 8-tetraethylpyrazino[2,3-g]quinoxaline-5,10-dione (600 mV) [48] and

benzo[b]phenazine-6,11-dione (400 mV) [49], indicating an improvement to the RTE, a parameter frequently overlooked in the ZIB literature. The average RTE value obtained from the experimental cycling of TBOBQ cathodes in this work was 90 %. As mentioned in the introduction, cathodes with low values of RTE can generate undesired heat, causing safety concerns such as thermal runaway and fire hazards [50]. The discharge capacity of the TBOBQ cathode can also be observed in Fig. 1c. TBOBQ-441 was cycled at a current density of 40 mA/g (C/4), delivering an initial discharge capacity of 147 mAh/g, followed by an increase to a maximum of 246 mAh/g after 4 cycles. After 4 charge/discharge cycles, the TBOBQ-441 electrode provided a discharge capacity in close agreement with the theoretical capacity of TBOBQ, calculated to be 243 mAh/g assuming a 2-electron reduction process occurring in each molecule (Supplementary discussion 2) within margins of error between the real and measured loading of active material in the electrodes. The increase in capacity observed over the first 4 charge/discharge cycles is attributed to progressive electrolyte penetration into the active material layer, resulting in an increased

**Table 1**

Comparative table of the discharge voltage at half-capacity, voltage hysteresis, discharge capacity, estimated energy density, capacity retention, and round-trip efficiency of different organic materials used as cathode materials in ZIBs.

Compound	Electrolyte	Discharge voltage [V vs Zn <sup>0</sup> /Zn <sup>2+</sup> ]	Voltage hysteresis [mV]	Discharge capacity [mAh/g]	Estimated energy density [Wh/kg] <sup>#</sup>	Capacity retention [%]	Round-trip efficiency [%]	Reference
3,5-di-tert-butyl-o-benzoquinone	1 M ZnSO <sub>4</sub>	1.1	100	246 at 40 mA/g	270	31 % after 1000 cycles at 100 mA/g	90	This work
2,3,7,8-tetraethylpyrazino[2,3-g] quinoxaline-5,10-dione	1 M ZnSO <sub>4</sub>	0.45	600	356 at 100 mA/g	160	25 % after 3000 cycles at 10 A/g	43*	[48]
p-chloranil	1 M Zn (OTf) <sub>2</sub>	1.1	~50	205 at 43 mA/g	226	34 % after 30 cycles at 43 mA/g	~95	[40]
Calix[4]quinone	3 M Zn (CF <sub>3</sub> SO <sub>3</sub> ) <sub>2</sub>	1.0	70	335 at 20 mA/g	335	33 % after 50 cycles at 100 mA/g	~93	[52]
3,4,9,10-perylene-tetracarboxylicacid-dianhydride	3 M Zn (CF <sub>3</sub> SO <sub>3</sub> ) <sub>2</sub>	0.4	300	315 at 100 mA/g	126	27 % after 15 cycles at 100 mA/g	57*	[46]
Poly(quinone-thiourea)	1 M ZnSO <sub>4</sub>	~0.9	~200	203 at 20 mA/g	183	83 % after 1000 cycles at 100 mA/g	82*	[53]
Poly(quinone-1,4-diaminoanthraquinone)	1 M Zn (CF <sub>3</sub> SO <sub>3</sub> ) <sub>2</sub>	0.78	~120	158 at 20 mA/g	123	72 % after 1000 cycles at 100 mA/g	87*	[54]
Pyrene-4,5,9,10-tetraone	2 M ZnSO <sub>4</sub>	0.7	~400	336 at 40 mA/g	235	70 % after 1000 cycles at 3 A/g	64*	[47]
Tetraamino-p-benzoquinone	1 M ZnSO <sub>4</sub>	~0.9	~120	303 at 100 mA/g	273	77 % after 1000 cycles at 5 A/g	88*	[21]
Dibenzo[b,i]thianthrene-5,7,12,14-tetraone	2 M ZnSO <sub>4</sub>	~0.76	140	211 at 50 mA/g	160	89 % after 150 cycles at 100 mA/g	84*	[55]
1,4,5,8-naphthalene diimide	2 M ZnSO <sub>4</sub>	0.51	290	240 at 100 mA/g	122	74 % after 2000 cycles at 1 A/g	64*	[56]
2,3-diaminophenazine	3 M Zn (CF <sub>3</sub> SO <sub>3</sub> ) <sub>2</sub>	0.6	150	219 at 255 mA/g (1 C)	131	80 % after 10,000 cycles at 1000 C	80*	[57]
Benz[i]benzo[6',7']quinoxalino [2',3':9,10]phenanthro[4,5-abc] phenazine-5,10,16,21-tetraone	2 M Zn (CF <sub>3</sub> SO <sub>3</sub> ) <sub>2</sub>	0.45	300	234 at 175 mA/g	105	74 % after 200 cycles at 175 mA/g	60*	[58]
Benzo[b]phenazine-6,11-dione	2 M ZnSO <sub>4</sub>	0.5	400	429 at 50 mA/g	214	73 % after 10,000 cycles at 5 A/g	55*	[49]
benzo [i] benzo [6,7] quinoxalino [2, 3-a] benzo [6,7] quinoxalino [2, 3-c] phenazine-5, 8, 13, 16, 21, 24-hexaone	2 M ZnSO <sub>4</sub>	~0.6	200	456 at 300 mA/g	274	66 % after 100 cycles at 300 mA/g	75*	[59]

#Estimated by the product of the reported discharge capacity and the discharge voltage

\*Estimated by [Discharge voltage / (Discharge voltage + voltage hysteresis)] \*100

proportion of the active material molecules being accessible to  $Zn^{2+}$  and  $H^+$  in the electrolyte [51]. The delivered capacity likely comes from the interaction between TBOBQ and the cations in the electrolyte ( $Zn^{2+}$  and  $H^+$ ) (Scheme 1), as the capacity of the acetylene black used as a conductive additive is negligible (Fig. S2). Based on the discharge curve in Fig. 1c with a discharge capacity of 246 mAh/g and a discharge voltage of 1.1 V vs  $Zn^0/Zn^{2+}$ , TBOBQ was observed to have an energy density of 270 Wh/kg. The energy density value was derived from the product of the discharge capacity and discharge voltage.

The impact of current density on the resulting charge and discharge characteristics of the TBOBQ cathodes is demonstrated in Fig. 1d. The

flat voltage plateaus in the charge and discharge curves showed negligible changes with increasing current densities, indicating fast electrochemical kinetics allowing the redox process to happen at high current densities, thereby resulting in maintained high energy densities [44,60]. Considering that TBOBQ is a non-conductive material, TBOBQ cathodes with different acetylene black contents were prepared and tested in coin cells to evaluate the dependency of capacity and rate capability on the content of conductive acetylene black. The capacity delivered by TBOBQ in the first discharge was reduced by 52 % when the acetylene black content in the slurry formulation was reduced from 45 wt% (199 mAh/g) in the TBOBQ-441 electrode to 10 wt% (103 mAh/g) in

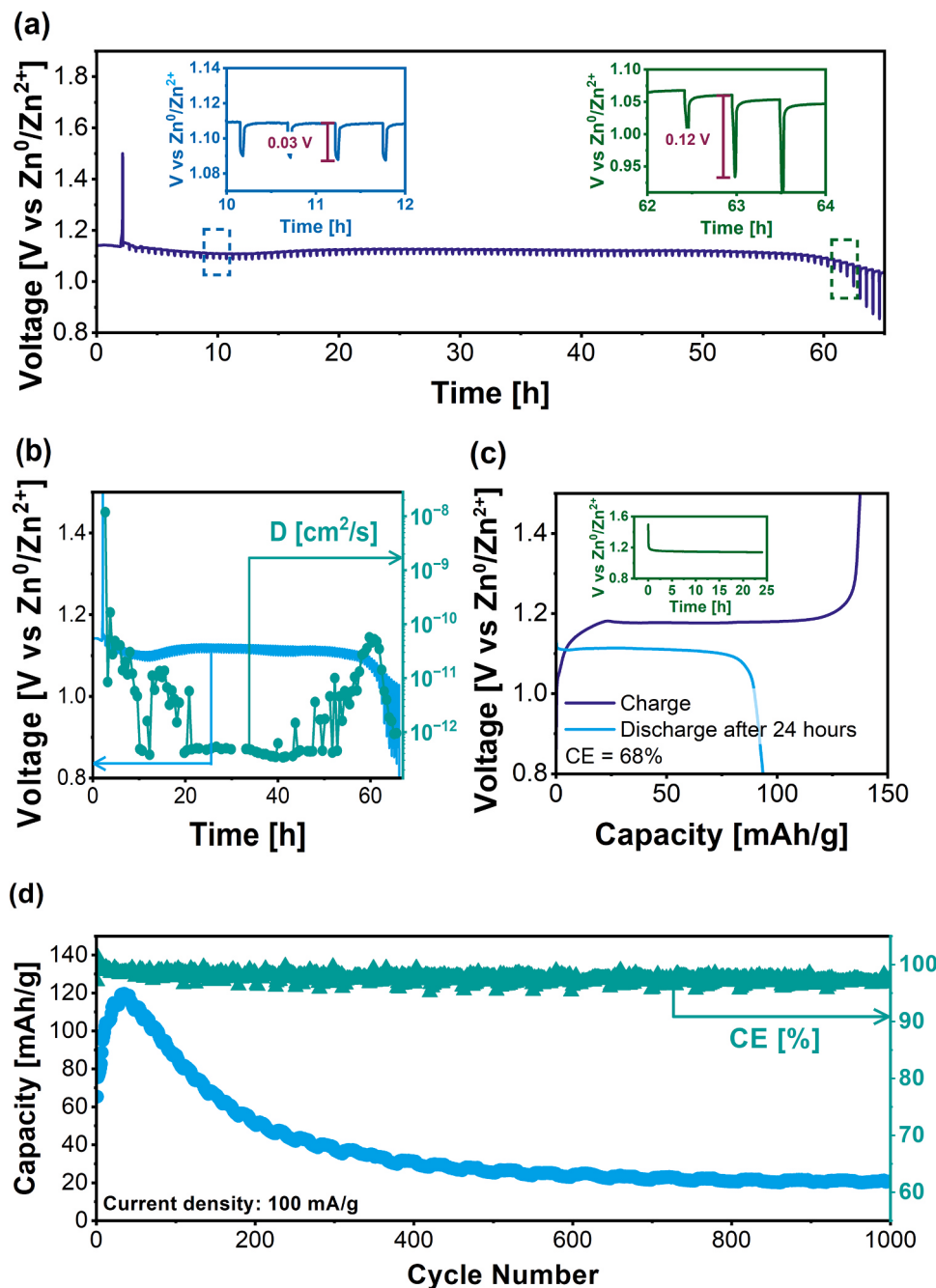


**Fig. 2.** Diffusion coefficient measurements, self-discharge behavior, and long-cycling performance of TBOBQ cathodes; (a) Evolution of cell voltage over time during GITT measurement. Insets highlight the overvoltage during the 30-minute rest time after individual current pulses of 40 mAh/g for 2 min. (b) GITT curve for the discharge titration (blue line) and value of the discharge diffusion coefficient at each titration stage (green dots). (c) Self-discharge test conducted at 40 mA/g of current density; first discharge curve to 0.8 V Vs  $Zn^0/Zn^{2+}$  after being charged to 1.5 V Vs  $Zn^0/Zn^{2+}$  and left to rest for 24 h at OCV. Inset: Voltage vs time curve at fully charged state. (d) Cycling performance and CE of the TBOBQ-441 electrode at 100 mA/g (C/2) of current density.

the TBOBQ-811 electrode (Fig. S3). Acetylene black increased the electrical conductivity of the cathode, as indicated by two-point probe resistance measurements (Table S1), which resulted in increased discharge capacity with higher acetylene black contents in the cathode. The increased electrical conductivity reflects more pathways for electron transport created by the increased proportion of acetylene black in the cathode configuration, resulting in a higher active material (*i.e.*, TBOBQ) utilization [61]. Furthermore, increased acetylene black content can provide a higher surface area for the uniform distribution of TBOBQ. Agglomerations of TBOBQ material in the electrode structure can block access of cations from the electrolyte and electrons from the current collector to the active material, making the isolated material inactive for energy storage [62]. A lower coulombic efficiency (CE) and capacity retention were achieved with higher acetylene black contents (Table S1). The low CE and capacity retention can be attributed to the increased surface area exposed to parasitic reactions with the electrolyte that the higher content of acetylene black provides [63]. Fig. 1e shows the rate capability test of TBOBQ cathodes with different acetylene black contents at current densities of 50 mA/g (C/4), 100 mA/g (C/2), 200 mA/g (1.34 C), 500 mA/g (3.5 C), and 1000 mA/g (7.8 C). At 500 mA/g, the TBOBQ-811 electrode delivered 58 % of the capacity shown at 50 mA/g, whereas TBOBQ-631 and TBOBQ-411 electrodes delivered 75 % and 70 %, respectively. When the current density was back to the initial value of 50 mA/g, the TBOBQ-411 cathode delivered a capacity similar to what was delivered at the beginning of the test (148 mAh/g).

EIS measurements of the three prepared cathodes (TBOBQ-411, TBOBQ-631, and TBOBQ-811) are displayed in Fig. S4. In the pristine cells, a decrease in the charge transfer resistance ( $R_{ct}$ ) when the content of acetylene black in the cathodes was increased was observed as indicated by the ratios of the semicircles in the high-frequency region of the Nyquist plot. Comparing the  $R_{ct}$  of cells at pristine stage and after 100 cycles, a decrease in the  $R_{ct}$  of 39 %, 64 %, and 74 % was also observed in the TBOBQ-811, TBOBQ-631, and TBOBQ-411 cathodes, respectively (Figs. 1f, S5, S6). The reduced  $R_{ct}$  can be attributed to increased wetting of the TBOBQ cathode with electrolyte as the battery cycles [64]. Another factor that could influence the reduction in  $R_{ct}$  during battery operation is the dissolution of TBOBQ material during discharge (discussed below), owing to the fact that TBOBQ is non-conductive.

The diffusion coefficient of the electrolyte cations into the cathode during charge and discharge was evaluated using GITT, as seen in Fig. 2a. During the first 50 h of the GITT measurement, the voltage of the battery using TBOBQ cathodes ranged between 1.1 V to 1.13 V vs  $Zn^0/Zn^{2+}$ , experiencing an overvoltage of 0.03 V after each current pulse. In the final 10 h of the GITT test, the overvoltage after the current pulse increased from 0.03 V to 0.12 V (Fig. 2a, inset). Sun *et al.* [65] attributed increasing overvoltage during the current pulses, as seen experimentally, to high diffusion resistances (*i.e.*, small diffusion coefficients) and slow-diffusing ions, due to their bulkiness and electrostatic forces (*e.g.*, solvated  $Zn^{2+}$ ), into the cathode. Analysis of the GITT data showed average cation diffusion coefficients of  $1.36 \times 10^{-10}$  and  $1.08 \times 10^{-11}$  cm<sup>2</sup>/s for the discharge and charge processes, respectively (Figs. 2b and S7). The calculated diffusion coefficients obtained from the TBOBQ cathodes were similar to other reported organic materials like poly(quinone-1,4-diaminoanthraquinone) ( $2.9 \times 10^{-11}$ -  $2.4 \times 10^{-10}$  cm<sup>2</sup>/s) [54]. The low wettability of the TBOBQ cathodes can increase the diffusion resistance of cations from the electrolyte into the cathode, which translates to low diffusion coefficients [66].

To evaluate the irreversible capacity loss from charged TBOBQ cathodes at OCV, self-discharge tests were performed. Self-discharge in organic electrode materials could be higher than in other types of materials and has been attributed to active material dissolution, voltage drops, and side reactions [67]. The capacity loss from the processes happening during self-discharge causes the value of CE to decrease from 100 %. During the self-discharge test, the battery was fully charged to 1.5 V vs  $Zn^0/Zn^{2+}$  and allowed to rest for a 24-hour period, where the

voltage decreased to an equilibrium value of 1.13 V  $Zn^0/Zn^{2+}$  (Fig. 2c, inset), showing a loss in voltage of 0.37 V. The subsequent discharge delivered a capacity of 93 mAh/g, which was 44 mAh/g less than the capacity provided in the prior charging step (137 mAh/g). Analyzing a charge/discharge curve where no rest period is present between charge and discharge (like the cycling protocol followed in Fig. 1c), a TBOBQ cathode delivers ca. 18 mAh/g of capacity between the top of charge voltage and the equilibrium voltage reached during the self-discharge test (1.5 to 1.13 V vs  $Zn^0/Zn^{2+}$ , Fig. S8). Hence, it can be inferred that 41 % of the 44 mAh/g (ca. 18 mAh/g) missing from the discharge capacity in the self-discharge test is lost due to the voltage decrease between 1.5 and 1.13 V vs  $Zn^0/Zn^{2+}$  during the rest period. The remaining 59 % (ca. 26 mAh/g) of discharge capacity missing in the self-discharge test is lost by other causes, such as the presence of parasitic side reactions involving the active material, which can produce new compounds [68], as discussed later. Additionally, the calculated CE of the self-discharge test was 68 %, also suggesting the presence of side reactions in the electrode that affect the capacity retention. Fig. S9 shows the self-discharge test of a TBOBQ cathode fully discharged to 0.8 V vs  $Zn^0/Zn^{2+}$ . The voltage loss during the rest time of the test, shown in Fig. S9, was 0.2 V (from 0.8 V to 1.0 V vs  $Zn^0/Zn^{2+}$ ). The charge capacity delivered after fully discharging and resting for 24 h was 10 mAh/g more than the discharged capacity in the previous step, indicating a slight self-discharge. The CE of the self-discharge test in Fig. S9 was calculated to be 93 %, being 25 % higher than the CE of the self-discharge test at fully charged state. The comparison of the CEs from the test shown in Fig. 2c and Fig. S9 suggested that the battery using TBOBQ as cathode loses less capacity when stored at the discharged state than when stored at the charged state.

The long-term cycling performance of the TBOBQ electrodes was investigated by performing 1000 charge/discharge cycles at a current density of 100 mA/g (C/2), with the results displayed in Fig. 2d. During the first 30 cycles of the long-term cycling test, the discharge capacity increased from 65 mAh/g to 120 mAh/g, which, as previously mentioned, could be attributed to an increased wetting of the cathode [51,69]. After the cell reached its maximum capacity, it could be observed a linear discharge capacity fade of approximately 1 mAh/g per cycle during the first 200 cycles, stabilizing at 21 mAh/g by cycle 600. The peak capacity of the cathode could be influenced by the ease of electrolyte permeation (which depends on hydrophilicity and porosity of the cathode) that gives access to cations for storage [69,70]. The capacity decay observed following the peak capacity could be attributed mainly to two mechanisms: dissolution of active material or active material degradation. As thoroughly discussed later, discharged TBOBQ cathodes showed evidence of decomposition reactions and dissolution during the discharge process. The capacity retention calculated based on the initial discharge capacity (65 mAh/g) and the maximum discharge capacity (120 mAh/g) was 31 % and 17 %, respectively, delivering a discharge capacity of 21 mAh/g after 1000 cycles. The capacity retained after the long-term test could be attributed to undecomposed TBOBQ material remaining in the cathode, given that the capacity provided by the acetylene black was negligible (Fig. S2). Additionally, a cyclic fluctuation of the discharge capacity could be observed during the long-term test. These fluctuations could be attributed to changes in the ambient temperature, given that the cells were not tested in a temperature chamber [71].

In addition to the voltage hysteresis and round-trip efficiency, Table 1 also compares the capacity retention of several organic cathode materials employed in ZIBs, along with the corresponding current density used during testing. When assessing cathode performance, it is valuable to utilize current densities that represent the operational conditions of the intended practical application of the energy storage system. In the context of stationary energy storage supporting renewable energy integration, C-rates in the range of C/4 to C/6 are considered most representative of real-world operational conditions [3]. As can be seen in Table 1, TBOBQ presented a similar capacity retention to other

organic materials tested at comparable current densities ( $\leq 100$  mA/g), like p-chloranil (34 % after 30 cycles at 43 mA/g) [40] and 3,4,9,10-perylene-tetracarboxylic acid-dianhydride (27 % after 15 cycles at 100 mA/g) [46]. However, Table 1 also revealed the necessity of improvements to be made with respect to the capacity retention of TBOBQ, particularly when compared to materials with lower discharge voltage, such as dibenzo[*b,i*]thianthrene-5,7,12,14-tetraone (89 % after 150 cycles at 100 mA/g) [55] and poly(quinone-thiourea) (83 % after 1000 cycles at 100 mA/g) [53]. Further studies of the energy storage and degradation mechanisms of TBOBQ cathodes will ideally lead to strategies for improving the capacity retention, hence allowing the leverage of the positive properties of TBOBQ, such as high discharge potential and small voltage hysteresis. Suggestions of strategies for enhancing the capacity retention of TBOBQ are discussed later.

FTIR was utilized to study the evolution of the carbonyl functional groups of TBOBQ going from the pristine state to the bottom of discharge at 0.8 V vs  $Zn^0/Zn^{2+}$  and then to the top of charge at 1.5 V vs  $Zn^0/Zn^{2+}$ , with the results shown in Fig. 3. In the 3 samples measured, peaks were observed at  $1622\text{ cm}^{-1}$  and  $1567\text{ cm}^{-1}$  (Fig. 3a), which are typically assigned to the carbon-carbon and carbon-oxygen double bonds of quinone structures [72]. When discharged, the intensity of the carbon-oxygen signals was attenuated, as shown by the dashed black arrows in Fig. 3a, indicating a reduction of the carbonyl structure. It is inferred that the carbonyl structure was transformed from  $C=O$  into  $C-O^-$ , where cations from the electrolyte can coordinate, compensating for the negative charge [21]. Thus, the carbonyl groups can be identified as the active sites for cation coordination and energy storage in the TBOBQ molecule. Furthermore, a recovery of the carbonyl signal was observed in the charged material spectra, indicated with the solid black arrows in Fig. 3a, indicating the reversibility of the cation coordination with the carbonyl groups [21,73]. Additionally, in the  $4000 - 2500\text{ cm}^{-1}$  range of the FTIR spectra (Fig. 3b), a broad peak at  $3336\text{ cm}^{-1}$  was observed in the spectra of the discharged and charged samples (solid black arrows in Fig. 3b). Broad signals at  $3500 - 3200\text{ cm}^{-1}$  are attributed to a hydroxyl group stretch [72], indicating a possible coordination of  $H^+$  with the reduced oxygen group.

SEM images of the surface of TBOBQ cathodes were taken after being exposed to several conditions relevant to ZIBs: after soaking in 1 M  $ZnSO_4$  electrolyte solution for 24 h (Fig. 4a), after first discharge to 0.8 V vs  $Zn^0/Zn^{2+}$  (Fig. 4b), after first charge to 1.5 V vs  $Zn^0/Zn^{2+}$  (Fig. 4c), and after second discharge to 0.8 V vs  $Zn^0/Zn^{2+}$  (Fig. 4d). All samples were rinsed thoroughly with Millipore Type I Ultrapure water to remove any  $ZnSO_4$  salt from the electrolyte used. After the first discharge, flake-shaped structures were observed on the TBOBQ electrode (Fig. 4b), which have been previously reported to correspond to

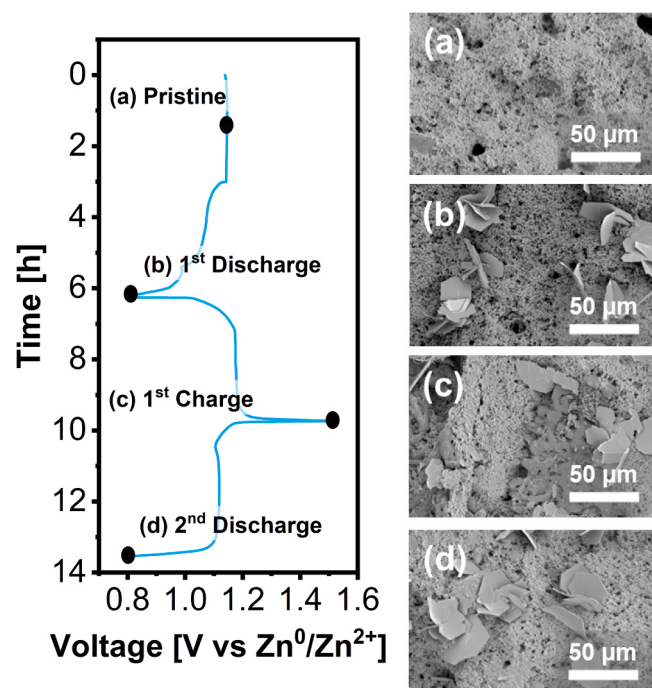


**Fig. 4.** SEM images of TBOBQ electrode samples at: (a) soaked electrode, (b) first discharge to 0.8 V vs  $Zn^0/Zn^{2+}$ , (c) first charge to 1.5 V vs  $Zn^0/Zn^{2+}$ , and (d) second discharge to 0.8 V vs  $Zn^0/Zn^{2+}$ .

zinc hydroxide sulfate (ZHS) on the surface of ZIB cathodes [74]. As reported in the literature [75], the ZHS structures are a product of the reaction of the zinc sulfate electrolyte with hydroxide ions, likely formed via the corrosion of the zinc anode, and/or the  $H^+$  uptake by the cathode.

Energy dispersive X-ray spectroscopy (EDS) was taken from the cathode after soaking in 1 M  $ZnSO_4$  electrolyte solution for 24 h (Fig. S10), after first discharge (Fig. S11), after first charge (Fig. S12), and after second discharge (Fig. S13). The EDS spectra of the TBOBQ electrode after first discharge (Fig. S11) showed that the flake structures are comprised of zinc. However, zinc was also present within the TBOBQ active material, indicating the coordination of  $Zn^{2+}$  with the carbonyl groups of TBOBQ during discharge. After the first charge, ZHS flakes were still observed on the TBOBQ electrode surface (Fig. 4c), though the atomic percentage of zinc decreased from 16 % to 7 % from the bottom of discharge to top of charge (Table S2). The reduction in the atomic

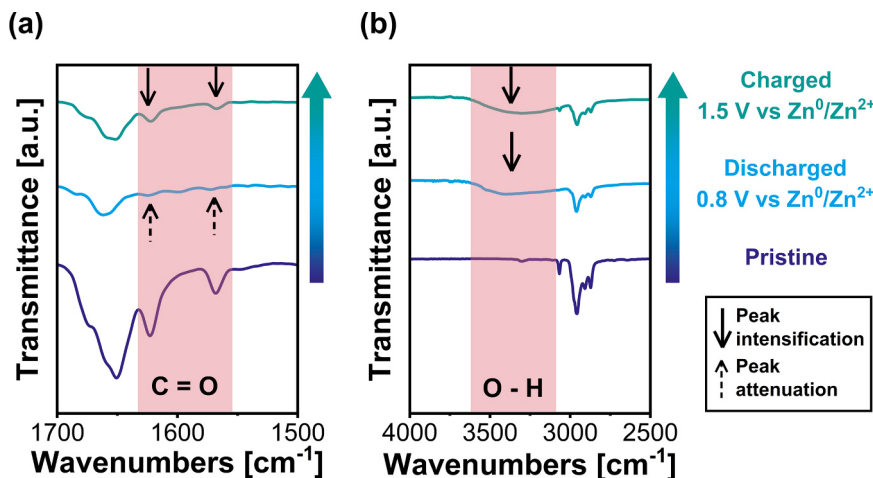


**Fig. 3.** Ex-situ FTIR spectra of TBOBQ electrode samples at pristine state, to bottom of discharge at 0.8 V vs  $Zn^0/Zn^{2+}$ , and to top of charge at 1.5 V vs  $Zn^0/Zn^{2+}$ ; (a)  $1700 - 1500\text{ cm}^{-1}$  wavelength and (b)  $4000 - 2500\text{ cm}^{-1}$  wavelength.

percentage of zinc at the top of charge indicates the removal of zinc from the TBOBQ cathodes, likely through the discoordination of  $Zn^{2+}$  from the carbonyl groups and the partial dissolution of ZHS flakes caused by the lower pH of the electrolyte created by the release of  $H^+$  from the cathode during charge. The SEM image of the TBOBQ cathode after the second discharge (Fig. 4d) showed an accumulation of ZHS flakes on the surface again and an increased weight percentage of zinc with respect to the values registered for the sample after first charge (Table S2).

XRD was performed on TBOBQ cathodes after being soaked in the 1 M  $ZnSO_4$  electrolyte solution for 24 h, after first discharge to 0.8 V vs  $Zn^0/Zn^{2+}$  and after first charge to 1.5 V vs  $Zn^0/Zn^{2+}$  (Fig. 5). The XRD after first discharge and first charge showed characteristic peaks of ZHS at  $2\theta = 8.5^\circ$  and  $17.3^\circ$  (PDF: 00-044-0673), further validating the identity of the flake structures seen in SEM. A consistent peak for monoclinic TBOBQ at  $2\theta = 13^\circ$  (PDF: 02-070-1379) was also present in the XRD spectrum of all the tested samples. The peak of the monoclinic TBOBQ stayed at the same  $2\theta$  value of  $13^\circ$  over the discharge and charge of the cathode, indicating no lattice expansion or contraction during discharge and charge, which suggests that the energy storage method is based on cation coordination with the functional groups of TBOBQ [76].

The material characterization done through SEM and XRD showing ZHS flakes suggests that the concentration of hydroxide ions increases at the electrode surface during discharge, with one possible reason being the participation of  $H^+$  in the energy storage mechanisms of the TBOBQ cathodes. These results indicate that local pH changes are likely happening during the TBOBQ charge/discharge mechanisms. To observe the pH variation in the electrolyte surrounding the TBOBQ cathode, pH measurements were performed in UV-Vis cuvette cells using an electrolyte containing bromocresol as a visual indicator, with the cathode being discharged and charged in the solution. As seen in Fig. S14, a change in coloration of the electrolyte from blue to yellow in the area surrounding the TBOBQ cathode at the top of charge was observed. The yellowish color of the bromocresol indicator denotes acidification of the electrolyte in the proximity of the TBOBQ cathode. The observed pH decrease suggests the release of  $H^+$  from the TBOBQ cathode during charge, which indicates some coordination of  $H^+$  with the carbonyl groups of TBOBQ during discharge. Nevertheless, the small pH variation observed suggests a low uptake of  $H^+$  during discharge. For elucidating the contribution of  $Zn^{2+}$  and  $H^+$  in the energy stored by TBOBQ during discharge, ICP-OES and CHNS-EA were used for measuring the content of zinc and sulfur, respectively. The complement of the zinc and sulfur measurements is necessary to understand the contribution of  $Zn^{2+}$  and  $H^+$ , given that the zinc present in the ZHS

structures does not contribute to the energy stored. As seen in Supplementary Discussion 3, the sole measurement of zinc showed that its content in the discharged cathode corresponds to 119.6 % of the equivalent zinc given the capacity discharged. These results do not account for the ZHS on the surface of the cathode observed in the SEM and XRD, making the calculations inaccurate. Hence, sulfur measurements of the discharged cathode account for the presence of ZHS, improving the analysis. Through ICP-OES and the weight of slurry used in the electrodes, the weight percentage of zinc was found to be 15.55 %, based on the weight of slurry of the cathode sample after discharge. On the other hand, CHNS-EA showed a weight percentage of 0.48 % of sulfur (based on the weight of slurry of the cathode sample after discharge), which can be related to the content of ZHS in the electrode sample. Through a series of mass balance calculations (Supplementary Discussions 4), it was found that the contribution of  $Zn^{2+}$  to the energy storage capacity through discharge was 2.9 times higher than the contribution of  $H^+$ . These results suggest the participation of both  $Zn^{2+}$  and  $H^+$  in the energy storage mechanism.

For further probing the role of  $Zn^{2+}$  in the energy storage mechanism, the pH measurement was repeated using 3,5-di-tert-butylcatechol (TBC), which is the reduced form of TBOBQ, as the cathode active material (Fig. 6). Literature shows that the oxidation of TBC releases  $H^+$  into the electrolyte, consequently causing a local pH decrease while producing TBOBQ in the process [77,78]. The charge/discharge curve of TBOBQ and TBC (Fig. S15) showed plateaus at similar voltage values (1.1 V and 1.2 V vs  $Zn^0/Zn^{2+}$  for discharge and charge, respectively), indicating similar electrochemical reactions happening in both materials. The pH measurements performed with TBC as cathode showed a yellowish coloration of the electrolyte at the interface with the cathode during charging (Fig. 6d), indicating a pH decrease to  $< 4$ . During the following discharge, the pH underwent a slow increase to values  $> 4$  that was observed close to the bottom of discharge, as described by the blue coloration of the bromocresol indicator in the electrolyte (Fig. 6f). The slow increase in pH during discharge can be attributed to a higher uptake of  $Zn^{2+}$  compared to  $H^+$  from the electrolyte, as indicated by ICP-OES and CHNS-EA, which keeps a high concentration of  $H^+$  in the electrolyte-electrode interphase, resulting in persistently low pH, observed as yellow coloration.

DFT calculations were also performed to further investigate the bonding mechanism of TBOBQ to  $Zn^{2+}$  and  $H^+$  atoms during the battery discharge. First, an ESP analysis was carried out for the TBOBQ molecule to identify the sites that could potentially coordinate with the cationic charge carriers in question ( $Zn^{2+}$  and  $H^+$ ). As can be seen in Fig. 7a, the highest electronic charge concentration (negative ESP values) in TBOBQ was identified around the carbonyl groups in ortho position, indicating that the carbonyl groups are likely active sites for cation uptake in TBOBQ. The  $Zn$ -TBOBQ and  $H_2$ -TBOBQ bonded structures were then created by coordinating one  $Zn^{2+}$  ion and two  $H^+$  ions to the carbonyl sites of TBOBQ, respectively. The geometry-optimized structure and the calculated binding energy ( $\Delta E_b$ ) of both  $Zn$ -TBOBQ and  $H_2$ -TBOBQ are shown in Fig. 7b. Both  $Zn$ -TBOBQ and  $H_2$ -TBOBQ report negative  $\Delta E_b$  values, demonstrating that the bonding of both cations to TBOBQ is predicted to be thermodynamically favorable. Therefore, it is thermodynamically feasible for both  $Zn^{2+}$  and  $H^+$  to participate in the energy storage mechanism of TBOBQ cathodes in aqueous rechargeable ZIBs, which is in agreement with the experimental results. However, it is important to note that the calculated  $\Delta E_b$  for  $H_2$ -TBOBQ (-20.9 eV) is considerably lower than for  $Zn$ -TBOBQ (-9.6 eV), which indicates a stronger binding of the two  $H^+$  ions to TBOBQ than of a single  $Zn^{2+}$  ion.

RRDE measurements were used to investigate the dissolution of TBOBQ during cycling (Fig. S16), with any dissolved TBOBQ material being pushed outwards by the rotation of the electrode and oxidized at the outer ring, generating a current [79]. In this work, an increase in the ring electrode current of  $1.14 \mu A$  was observed starting at a disk electrode potential of 1.04 V vs  $Zn^0/Zn^{2+}$  until the end of discharge at 0.8 V  $Zn^0/Zn^{2+}$ . The total charge registered in the ring during the experiment

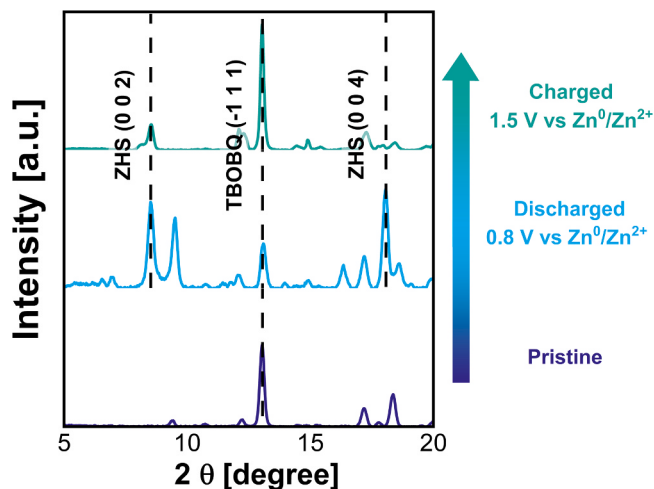


**Fig. 5.** XRD patterns of TBOBQ electrode samples after soaking for 24 h in 1 M  $ZnSO_4$  electrolyte, after the first discharge to 0.8 V vs  $Zn^0/Zn^{2+}$ , after the first charge to 1.5 V vs  $Zn^0/Zn^{2+}$ .

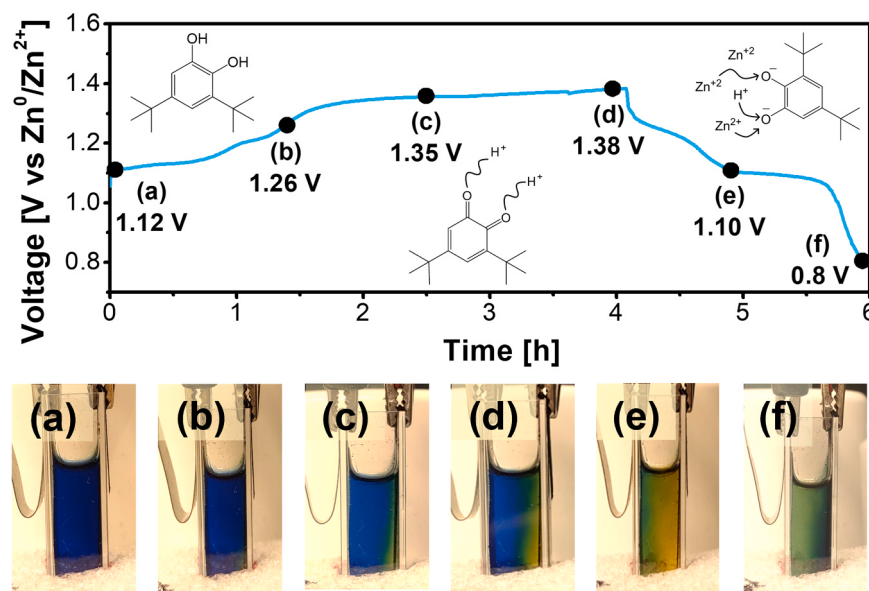


**Fig. 6.** pH measurements in a UV-vis cuvette of a TBC cathode (right wall of the cell) and metallic zinc anode (left wall of the cell) in 1 M ZnSO<sub>4</sub> using bromocresol at different cycle stages and the cell voltage of each picture. Blue: pH > 5.4; green: pH = 4.5; yellow: pH < 4.

was 301.86 µC, as calculated from the area under the curve of the detected ring current, as shown in Fig. S17. The total charge detected in the ring indicated a dissolution of 1.38 µg of TBOBQ (**Supplementary Discussion 5**), representing 1.3 % of the disk loading. The dissolution of TBOBQ can contribute to lowering the R<sub>ct</sub> of the cathode, as observed in the EIS measurements of Figs. 1f, S5, and S6, as a lower portion of insulating materials (i.e., TBOBQ) remains in the electrode.

The specific chemical species present in the cathode during charge and discharge were detected through liquid <sup>1</sup>H NMR and GC/MS of TBOBQ extracted from the cycled cathodes. The <sup>1</sup>H NMR spectra of a cathode after the first discharge showed a peak at 1.2 ppm that corresponds to the tertbutyl groups of TBOBQ (Fig. S18). The peaks observed at 6.1 and 7 ppm are associated with the aromatic ring in TBOBQ (Fig. S18, inset), indicating the presence of pristine TBOBQ in the discharged state of the cathode. Peaks at 7.1, 7.2, 7.75, and 9.1 ppm were also observed in the <sup>1</sup>H NMR spectra (Fig. S18, inset), indicating that TBC is one of the products in the discharged cathode. The presence of TBC in the discharged cathode indicated that H<sup>+</sup> was one type of charge carrier during battery operation, in accordance with the SEM, XRD, and electrolyte pH measurements. Additionally, unidentified resonances at 9.6 ppm and 10.2 ppm were observed (Fig. S18, inset, Fig. S19). The unknown resonances observed can possibly be attributed to carboxylic acids or aldehyde groups, indicating a possible ring-opening process of the TBOBQ molecule. Specifically, the broadness of the peak at 9.6 ppm is indicative of a carboxylic acid. As a result of the appearance of the unidentified resonances at 9.6 ppm and 10.2 ppm, the presence of byproducts caused by parasitic reactions in the TBOBQ cathode during cycling can be inferred. Studies of the degradation of different organic compounds, including quinones, in energy storage devices have previously reported following pathways such as nucleophilic addition, tautomerization, and ring-opening [80,81]. During the electrochemical reduction and oxidation of quinones, the formation of highly reactive semiquinone radicals can be observed when the electrochemical reaction happens in two or more electron transfer steps, like the process shown schematically in Fig. S20. The highly reactive semiquinone radicals can be prone to parasitic reactions with the electrolyte or with themselves [18,77]. Focusing on the TBOBQ-TBC couple, Hassanein *et al.* reported the oxidative ring cleavage of TBOBQ by hydroxyl radicals when chemically oxidizing TBC into TBOBQ in aqueous media [78]. The oxidative ring cleavage of TBOBQ during cycling can be related to the unidentified peaks at 9.6 and 10.2 ppm in the <sup>1</sup>H NMR spectra.

For elucidating more properties of the products formed in the TBOBQ cathode after battery discharge, GC/MS was employed. The spectra obtained from a discharged TBOBQ cathode detected the presence of the pristine TBOBQ molecule (Fig. S21) and TBC (Fig. S22), consistent with the results demonstrated by <sup>1</sup>H NMR. The GC/MS also showed compounds with molecular weights higher than the original TBOBQ or TBC molecules. Fig. S23 shows that compounds with molecular weights ranging from 226.2 to 377.1 g/mol were detected at 10.2, 12.4, and 12.8 min. Since the molecular weight of the compounds found in Fig. S23 does not correspond to multiples of the molecular weight of TBOBQ (220.3 g/mol), the detected compounds are likely fractional dimers of TBOBQ. The dimerization of quinone materials in batteries has been previously reported through extensive NMR studies [23]. The quinone radical intermediates are highly likely to be involved in dimer-forming reactions due to their high reactivity [18,81].

The material characterization of TBOBQ cathodes after repeated cycling showed dissolution during discharge as well as decomposition reactions that underpin the observed capacity fade. One strategy for suppressing the causes of capacity fade mentioned before is using TBOBQ as a building block for a macromolecule, as done by Nam *et al.* [22] with a triangular phenanthrenequinone macrocycle. The increased molecular weight could inhibit active material dissolution, and the extension of the conjugated structure could reduce the reactivity of radicals formed during cycling, protecting the active material from decomposition reactions [2]. Alternatively, grafting TBOBQ to a conductive carbon substrate could benefit the electrical conductivity of the cathode and reduce the dissolution, as shown previously in the case of Jaffe *et al.* [45]. Finally, the mass loadings used in this paper were low in order to evaluate the intrinsic energy storage capabilities of TBOBQ as cathode active material in aqueous rechargeable ZIBs. It is important to note that, upon discovery of a promising organic active material, the next challenge is to incorporate these materials into a high-loading, densely packed electrode with effective electron and ion transport. The transition from bench scale to practical applications is further discussed in our previous perspective paper [3].

## Conclusions

In this work, TBOBQ was investigated for use as an organic cathode in next-generation aqueous rechargeable zinc-ion batteries. The charge/discharge curves showed that the TBOBQ-441 cathodes, prepared with

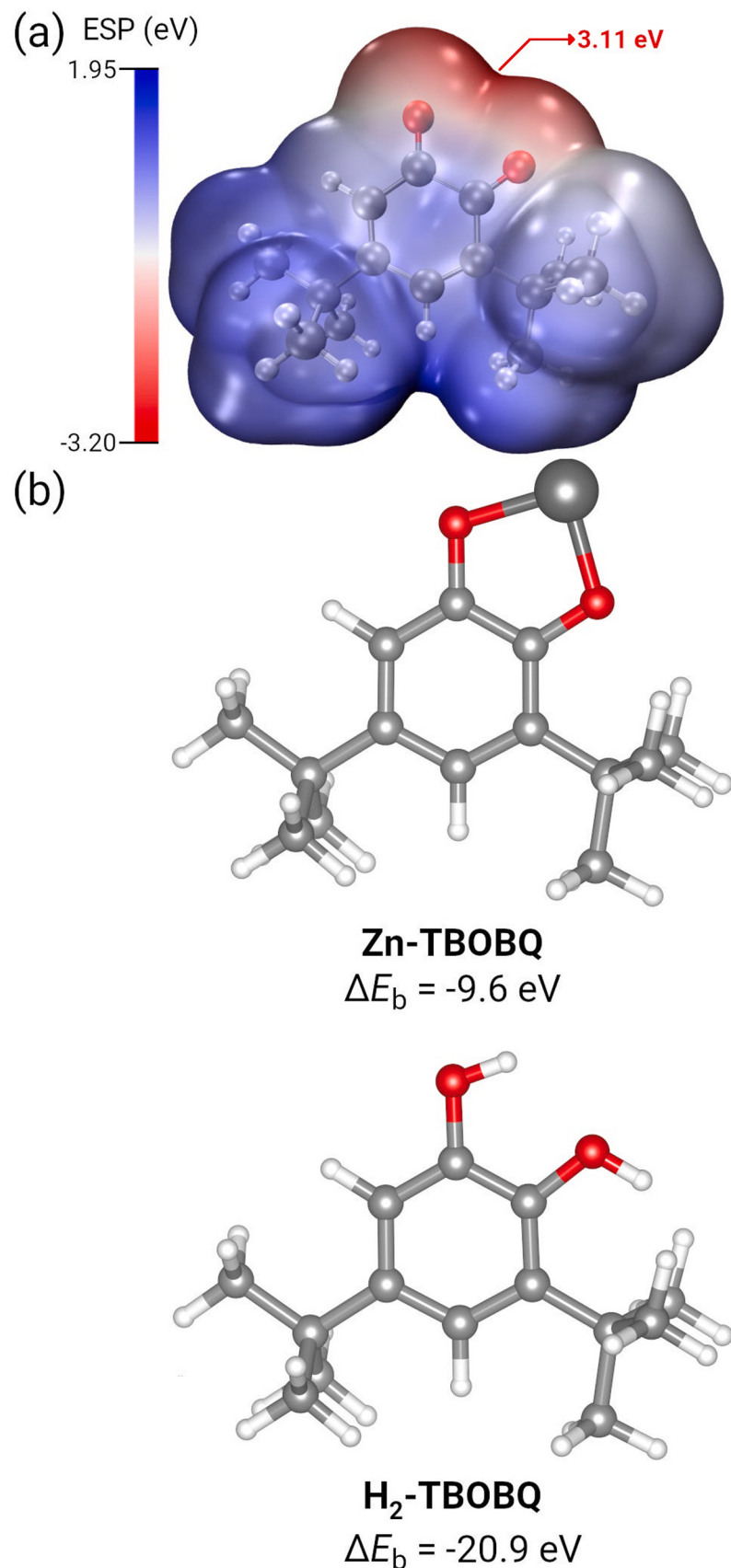


**Fig. 7.** (a) Calculated ESP for the TBOBQ molecule. (b) Geometry-optimized structure and binding energy ( $\Delta E_b$ ) of one  $\text{Zn}^{2+}$  ( $\text{Zn-TBOBQ}$ ) and two  $\text{H}^+$  ( $\text{H}_2\text{-TBOBQ}$ ) bonded to TBOBQ.

TBOBQ, acetylene black, and PVDF in a weight ratio of 45:45:10, delivered a high discharge capacity of 246 mAh/g at 40 mA/g, reaching the theoretical capacity (243 mAh/g) of a 2-electron reduction of TBOBQ, within margins of error between the real and measured loading of active material in the electrodes. The voltage hysteresis of only 100 mV between the voltage plateaus on charge and discharge led to an average RTE of 90 %. Long-term cycling of TBOBQ showed a linear capacity fade of approximately 1 mAh/g per cycle during the first 200 cycles, retaining ca. 31 % of the initial capacity by cycle 1000. Regarding the energy storage mechanism, FTIR indicated the carbonyl functional groups as the main redox center of the molecule based on the carbonyl group signals during cycling. Through ICP-OES and CHNS-EA the weight percentage of Zn<sup>2+</sup> and S, respectively, were measured. Using mass balance calculations, the contribution of Zn<sup>2+</sup> to the energy stored was calculated to be 2.9 times bigger than the H<sup>+</sup> contribution. XRD showed no lattice expansion of the TBOBQ crystal, indicating no cation insertion in the structure, and instead, the energy storage relied on the redox activity of the electrochemically active functional groups present in the TBOBQ molecules. <sup>1</sup>H NMR and GC-MS detected TBC as one of the compounds present in the discharged TBOBQ cathode alongside the presence of degradation products, tentatively aldehydes or carboxylic acids of molecular weight ranging from 226.2 to 377.1 g/mol. This study lays the groundwork for future scientific developments in the field of aqueous ZIBs using TBOBQ, specifically on the energy storage mechanism and degradation pathways, that will contribute towards the commercialization of safe and reliable grid energy storage.

#### CRediT authorship contribution statement

**Alejandra Ibarra Espinoza:** Writing – original draft, Visualization, Methodology, Investigation, Formal analysis, Conceptualization. **Thomas J. Baker:** Writing – review & editing, Investigation, Formal analysis. **Storm W. D. Gourley:** Writing – review & editing, Investigation. **Caio M. Miliante:** Writing – review & editing, Visualization, Methodology, Formal analysis. **Kevin J. Sanders:** Investigation, Formal analysis. **Zeyuan Liu:** Formal analysis. **Gillian R. Goward:** Supervision, Formal analysis, Conceptualization. **Oleg Rubel:** Supervision, Formal analysis. **Brian D. Adams:** Writing – review & editing, Methodology, Funding acquisition, Conceptualization. **Drew Higgins:** Writing – review & editing, Supervision, Funding acquisition, Conceptualization.

#### Funding

This work was supported by the Natural Sciences and Engineering Research Council of Canada (NSERC) Alliance program; Salient Energy Inc., Ontario Graduate Scholarship (OGS); and the NSERC Canada Graduate Scholarship Doctoral program.

#### Declaration of Competing Interest

B.D.A is co-founder and partial owner of Salient Energy Inc. Salient Energy Inc. is developing and commercializing ZIB technology. The work disclosed in this manuscript is protected through a United States Provisional Patent Application.

#### Acknowledgments

Financial support for this work was provided by the Natural Sciences and Engineering Research Council of Canada (NSERC) Alliance program and Salient Energy Inc. TJB acknowledges support from the Ontario Graduate Scholarship (OGS) program, and SWDG acknowledges support from the NSERC Canada Graduate Scholarship Doctoral program. CMM acknowledges the support provided by the Digital Research Alliance of Canada (alliancecan.ca) and Gaussian Inc. (gaussian.com) in performing the theoretical calculations presented in this paper. All electron microscopy measurements were performed at the Canadian Center for

Electron Microscopy (CCEM), NMR measurements were conducted at the McMaster Nuclear Magnetic Resonance Facility, Gas chromatography-mass spectroscopy measurements were conducted at the McMaster Regional Centre for Mass Spectrometry (MRCMC), and X-ray diffraction measurements were conducted at the McMaster Analytical X-ray Diffraction Facility (MAX), all of which are at McMaster University.

#### Appendix A. Supporting information

Supplementary data associated with this article can be found in the online version at doi:10.1016/j.fub.2025.100092.

#### Data Availability

Data will be made available on request.

#### References

- [1] T.M. Gür, Energy amp Environ. Sci. 11 (10) (2018) 2696–2767, <https://doi.org/10.1039/c8ee01419a>.
- [2] P. Poizot, J. Gaubicher, S. Renault, L. Dubois, Y. Liang, Y. Yao, Chem. Rev. 120 (14) (2020) 6490–6557, <https://doi.org/10.1021/acs.chemrev.9b00482>.
- [3] S.W.D. Gourley, R. Brown, B.D. Adams, D. Higgins, Joule 7 (7) (2023) 1415–1436, <https://doi.org/10.1016/j.joule.2023.06.007>, 2023/07/19/.
- [4] P. He, et al., EnergyChem 1 (3) (2019) 100022, <https://doi.org/10.1016/j.enchem.2019.100022>, 2019/11/01/.
- [5] L.E. Blanc, D. Kundu, L.F. Nazar, Joule 4 (4) (2020) 771–799, <https://doi.org/10.1016/j.joule.2020.03.002>, 2020/04/15/.
- [6] M.R. Dunkin, et al., Adv. Mater. Interfaces 9 (29) (2022) 2201125, <https://doi.org/10.1002/admi.202201125>.
- [7] Y.-P. Deng, R. Liang, G. Jiang, Y. Jiang, A. Yu, Z. Chen, ACS Energy Lett. 5 (5) (2020) 1665–1675, <https://doi.org/10.1021/acsnenergylett.0c00502>, 2020/05/08/.
- [8] H. Pan, et al., Nat. Energy 1 (5) (2016) 16039, <https://doi.org/10.1038/nenergy.2016.39>, 2016/04/18/.
- [9] D. Kundu, B.D. Adams, V. Duffort, S.H. Vajargah, L.F. Nazar, Nat. Energy 1 (10) (2016) 16119, <https://doi.org/10.1038/nenergy.2016.119>, 2016/08/26/.
- [10] L. Wang, et al., Adv. Mater. Interfaces 8 (9) (2021) 2002080, <https://doi.org/10.1002/admi.202002080>.
- [11] G. Sampardi, F. La Mantia, Curr. Opin. Electrochem. 21 (2020) 84–92, <https://doi.org/10.1016/j.coelec.2020.01.014>, 2020/06/01/.
- [12] L. Li, et al., Ionics 28 (1) (2022) 283–293, <https://doi.org/10.1007/s11581-021-04304-6>.
- [13] D. Wu, et al., Energy amp Environ. Sci. 13 (11) (2020) 4322–4333, <https://doi.org/10.1039/d0ee02168g>.
- [14] A.M. Alfaraidi, et al., ACS Appl. Energy Mater. 6 (24) (2023) 12259–12266, <https://doi.org/10.1021/acsadm.3c01943>.
- [15] Z. Ye, et al., Energy Storage Mater. 37 (2021) 378–386, <https://doi.org/10.1016/j.ensm.2021.02.022>.
- [16] Y. Hu, et al., Adv. Funct. Mater. 30 (17) (2020) 2000675, <https://doi.org/10.1002/adfm.202000675>.
- [17] S.Y. An, T.B. Schon, B.T. McAllister, D.S. Seferos, EcoMat 2 (4) (2020) e12055, <https://doi.org/10.1002/eom2.12055>, 2020/12/01/.
- [18] Y. Lu, Q. Zhang, J. Chen, CCS Chem. 5 (7) (2023) 1491–1508, <https://doi.org/10.31635/ccschem.023.202302740>.
- [19] E.J. Son, J.H. Kim, K. Kim, C.B. Park, J. Mater. Chem. A 4 (29) (2016) 11179–11202, <https://doi.org/10.1039/C6TA03123D>.
- [20] Y. Ding, C. Zhang, L. Zhang, Y. Zhou, G. Yu, Chem. Soc. Rev. 47 (1) (2018) 69–103, <https://doi.org/10.1039/C7CS00569E>.
- [21] Z. Lin, H.-Y. Shi, L. Lin, X. Yang, W. Wu, X. Sun, Nat. Commun. 12 (1) (2021) 4424, <https://doi.org/10.1038/s41467-021-24701-9>, 2021/07/20/.
- [22] K.W. Nam, H. Kim, Y. Beldjoudi, T.-w Kwon, D.J. Kim, J.F. Stoddart, J. Am. Chem. Soc. 142 (5) (2020) 2541–2548, <https://doi.org/10.1021/jacs.9b12436>, 2020/02/05/.
- [23] Y. Jing, et al., Nat. Chem. 14 (10) (2022) 1103–1109, <https://doi.org/10.1038/s41557-022-00967-4>, 2022/10/01/.
- [24] E. Grignon, A.M. Battaglia, T.B. Schon, D.S. Seferos, iScience 25 (5) (2022) 104204, <https://doi.org/10.1016/j.isci.2022.104204>, 2022/05/20/.
- [25] Y. Lu, Q. Zhang, L. Li, Z. Niú, J. Chen, Chem 4 (12) (2018) 2786–2813, <https://doi.org/10.1016/j.chempr.2018.09.005>, 2018/12/13/.
- [26] K. Park, et al., ACS Sustain. Chem. Eng. 9 (24) (2021) 8214–8221, <https://doi.org/10.1021/acssuschemeng.1c02133>, 2021/06/21/.
- [27] A. Eftekhari, Sustain. Energy amp Fuels 1 (10) (2017) 2053–2060, <https://doi.org/10.1039/c7se00350a>.
- [28] B. Yang, Y. Ma, D. Bin, H. Lu, Y. Xia, ACS Appl. Mater. amp Interfaces 13 (49) (2021) 58818–58826, <https://doi.org/10.1021/acsami.1c20087>.
- [29] X. Cui, Y. Zhang, J. Zhang, E. Xie, J. Fu, Adv. Mater. Technol. (2023), <https://doi.org/10.1002/admt.202300321>.
- [30] Gaussian 16 Rev. C.01. (2016). Wallingford, CT.

- [31] A.D. Becke, J. Chem. Phys. 98 (7) (1993) 5648–5652, <https://doi.org/10.1063/1.464913>.
- [32] A.D. McLean, G.S. Chandler, J. Chem. Phys. 72 (10) (1980) 5639–5648, <https://doi.org/10.1063/1.438980>.
- [33] R. Krishnan, J.S. Binkley, R. Seeger, J.A. Pople, J. Chem. Phys. 72 (1) (1980) 650–654, <https://doi.org/10.1063/1.438955>.
- [34] A.V. Marenich, C.J. Cramer, D.G. Truhlar, J. Phys. Chem. B 113 (18) (2009) 6378–6396, <https://doi.org/10.1021/jp810292n>, 2009/05/07.
- [35] T. Lu, F. Chen, J. Comput. Chem. 33 (5) (2012) 580–592, <https://doi.org/10.1002/jcc.22885>.
- [36] J. Zhang, J. Chem. Theory Comput. 14 (2) (2018) 572–587, <https://doi.org/10.1021/acs.jctc.7b00788>, 2018/02/13.
- [37] W. Humphrey, A. Dalke, K. Schulten, J. Mol. Graph. 14 (1) (1996) 33–38, [https://doi.org/10.1016/0263-7855\(96\)00018-5](https://doi.org/10.1016/0263-7855(96)00018-5), 1996/02/01/.
- [38] J. Xie, et al., Front. Chem. Sci. Eng. 17 (2) (2023) 217–225, <https://doi.org/10.1007/s11705-022-2214-7>.
- [39] X. Xiao, T. Wang, Y. Zhao, W. Gao, S. Wang, J. Colloid Interface Sci. 642 (2023) 340–350, <https://doi.org/10.1016/j.jcis.2023.03.164>, 2023/07/15/.
- [40] D. Kundu, et al., Chem. Mater. 30 (11) (2018) 3874–3881, <https://doi.org/10.1021/acs.chemmater.8b01317>, 2018/06/12.
- [41] P. Simon, Y. Gogotsi, B. Dunn, Science 343 (6176) (2014) 1210–1211, <https://doi.org/10.1126/science.1249625>.
- [42] S. Fleischmann, et al., Chem. Rev. 120 (14) (2020) 6738–6782, <https://doi.org/10.1021/acs.chemrev.0c00170>, 2020/07/22.
- [43] J.F. Rusling, S.L. Suib, Adv. Mater. 6 (12) (1994) 922–930, <https://doi.org/10.1002/adma.19940061204>.
- [44] C.N. Gannett, L. Melecio-Zambrano, M.J. Theibault, B.M. Peterson, B.P. Fors, H. D. Abruna, Mater. Rep. Energy 1 (1) (2021) 100008, <https://doi.org/10.1016/j.matre.2021.01.003>, 2021/02/01/.
- [45] A. Jaffe, A. Saldivar Valdes, H.I. Karunadasa, Chem. Mater. 27 (10) (2015) 3568–3571, <https://doi.org/10.1021/acs.chemmater.5b00990>, 2015/05/26.
- [46] X. Gao, et al., Electrochim. Acta 453 (2023) 142321, <https://doi.org/10.1016/j.electacta.2023.142321>, 2023/06/10/.
- [47] Z. Guo, Y. Ma, X. Dong, J. Huang, Y. Wang, Y. Xia, Angew. Chem. Int. Ed. 57 (36) (2018) 11737–11741, <https://doi.org/10.1002/anie.201807121>.
- [48] Y. Shi, et al., Mater. Lett. 384 (2025) 138062, <https://doi.org/10.1016/j.matlet.2025.138062>, 2025/04/01/.
- [49] Y. Shi, et al., Chem. Eng. J. (2023) 141850, <https://doi.org/10.1016/j.cej.2023.141850>, 2023/02/11/.
- [50] X. Yang, A.L. Rogach, Adv. Energy Mater. 9 (25) (2019) 1900747, <https://doi.org/10.1002/aenm.201900747>, 2019/07/01.
- [51] H. Gao, et al., J. Am. Chem. Soc. 144 (21) (2022) 9434–9442, <https://doi.org/10.1021/jacs.2c02196>.
- [52] Q. Zhao, et al., Sci. Adv. 4 (3) (2018) eaao1761, <https://doi.org/10.1126/sciadv.aao1761>.
- [53] C. Guo, Y. Liu, L. Wang, D. Kong, J. Wang, ACS Sustain. Chem. Eng. 10 (1) (2022) 213–223, <https://doi.org/10.1021/acssuschemeng.1c05881>.
- [54] C. Guo, et al., Ionics (2023), <https://doi.org/10.1007/s11581-023-04980-6>.
- [55] Y. Wang, et al., Adv. Mater. 32 (16) (2020) 2000338, <https://doi.org/10.1002/adma.202000338>.
- [56] X. Wang, L. Chen, F. Lu, J. Liu, X. Chen, G. Shao, ChemElectroChem 6 (14) (2019) 3644–3647, <https://doi.org/10.1002/celc.201900750>.
- [57] J. Liang, et al., J. Colloid Interface Sci. 607 (2022) 1262–1268, <https://doi.org/10.1016/j.jcis.2021.09.072>.
- [58] T. Sun, Z. Yi, W. Zhang, Q. Nian, H.J. Fan, Z. Tao, Adv. Funct. Mater. (2023), <https://doi.org/10.1002/adfm.202306675>.
- [59] Y. An, Y. Liu, S. Tan, F. Xiong, X. Liao, Q. An, Electrochim. Acta 404 (2022) 139620, <https://doi.org/10.1016/j.electacta.2021.139620>.
- [60] S. Maiti, et al., Energy Storage Mater. 56 (2023) 25–39, <https://doi.org/10.1016/j.ensm.2023.01.004>, 2023/02/01/.
- [61] C. Tomon, et al., Commun. Chem. 5 (1) (2022) 54, <https://doi.org/10.1038/s42004-022-00670-y>.
- [62] T. Tomai, H. Hyodo, D. Komatsu, I. Honma, J. Phys. Chem. C. 122 (5) (2018) 2461–2466, <https://doi.org/10.1021/acs.jpcc.7b08124>.
- [63] T. Marks, S. Trussler, A.J. Smith, D. Xiong, J.R. Dahn, J. Electrochem. Soc. 158 (1) (2011) A51, <https://doi.org/10.1149/1.3515072>, 2010/11/29.
- [64] Y.-F. Li, et al., Adv. Sci. 8 (14) (2021) 2100911, <https://doi.org/10.1002/advs.202100911>.
- [65] W. Sun, et al., J. Am. Chem. Soc. 139 (29) (2017) 9775–9778, <https://doi.org/10.1021/jacs.7b04471>.
- [66] J. Hao, et al., Adv. Funct. Mater. 29 (34) (2019) 1903605, <https://doi.org/10.1002/adfm.201903605>.
- [67] B. Babu, Energy Storage Mater. 67 (2024) 103261, <https://doi.org/10.1016/j.ensm.2024.103261>.
- [68] M.-A. Goulet, M.J. Aziz, J. Electrochem. Soc. 165 (7) (2018) A1466–A1477, <https://doi.org/10.1149/2.0891807jes>.
- [69] D.H. Jeon, Energy Storage Mater. 18 (2019) 139–147, <https://doi.org/10.1016/j.ensm.2019.01.002>.
- [70] F. Chen, et al., Green. Energy Intell. Transp. 4 (1) (2025) 100248, <https://doi.org/10.1016/j.geits.2024.100248>.
- [71] M.A. Fatullah, A. Rahardjo, F. Husnayain, 2019 IEEE Int. Conf. Innov. Res. Dev. (ICIRD) 28-30 (2019) 1–5, <https://doi.org/10.1109/ICIRD47319.2019.9074667>.
- [72] A.B.D. Nandiyanto, R. Oktiani, R. Ragadhitia, 2019 FTIR Infrared Spectr. Org. Mater. Chem. Bond Org. Struct. 4 (1) (2019) 22, <https://doi.org/10.17509/ijost.v4i1.15806>, 2019-03-07.
- [73] H. Dong, et al., J. Phys. Chem. C. 125 (38) (2021) 20814–20820, <https://doi.org/10.1021/acs.jpcc.1c06870>, 2021/09/30.
- [74] S. Zhao, et al., J. Mater. Chem. A 6 (14) (2018) 5733–5739, <https://doi.org/10.1039/c8ta01031e>.
- [75] H. Chen, et al., Adv. Mater. 34 (15) (2022) 2109092, <https://doi.org/10.1002/adma.202109092>.
- [76] I.R. Tay, J. Xue, W.S.V. Lee, Adv. Sci. 10 (26) (2023) 2303211, <https://doi.org/10.1002/advs.202303211>.
- [77] A. Zahirović, E. Kahravić, Mon. F. üR. Chem. Chem. Mon. 152 (10) (2021) 1193–1200, <https://doi.org/10.1007/s00706-021-02842-3>.
- [78] M. Hassanein, S.E.-D.H. Etaïw, S.H. El-Khalafy, M.M. El-Bendary, J. Inorg. Organomet. Polym. Mater. 25 (4) (2015) 664–670, <https://doi.org/10.1007/s10904-014-0139-4>.
- [79] J. Zheng, Y. Geping, J. Zhang, Rotating Ring-disk Electrode Method. Rotating electrode methods and oxygen reduction electrocatalysts, Elsevier, 2014, pp. 199–229, ch. 6.
- [80] Y. Liu, et al., Curr. Opin. Electrochem. 32 (2022) 100895, <https://doi.org/10.1016/j.coelec.2021.100895>.
- [81] M.-A. Goulet, et al., J. Am. Chem. Soc. 141 (20) (2019) 8014–8019, <https://doi.org/10.1021/jacs.8b13295>, 2019/05/22.